Hindawi
Advances in Civil Engineering
Volume 2018, Article ID 5748278, 9 pages
https://doi.org/10.1155/2018/5748278

Research Article

Research of Steel-Concrete Composite Bridge under Blasting Loads

Yuan Li and Shuanhai He

School of Highway, Chang'an University, Xi'an 710064, China

Correspondence should be addressed to Yuan Li; liyuan@chd.edu.cn

Received 16 April 2018; Revised 25 June 2018; Accepted 5 August 2018; Published 12 September 2018

Academic Editor: Xihong Zhang

This paper presents a study to simulate the performance of steel-plate composite bridge under various blasting loads. The multi-Euler domain method based on the fully coupled Lagrange and Euler models is adopted for the structural analysis of explosion process with the commercial software Autodyn. Due to the difference of material characteristics and space distribution between the concrete and steel part, the most adverse position is estimated to be above and below detonation. A remarkable difference between these two explosive denotations for steel-concrete composite bridge is noted, and the failure mode above denotation is the damage of local concrete deck, with the compression mode near the denotation point showing a standard trigonometric curve. The failure mode below denotation includes damage of steel girders and concrete failure near junction.

1. Introduction

Blasting incidents are becoming an increasing threat for urban infrastructure in the past years. Terrorist attacks and transport vehicles with explosive and flammable materials cause potential blasting loads structures subjected to. Terrorism and accidental explosion have become a major threat to the security of international community. As crucial thoroughfare for urban traffic system, disastrous bridge failures can bring enormous economic and related loss especially in populated regions. Bridge engineers are focused on bridge antiexplosion and blasting damage assessment especially after the incident of 911. However, consideration of prominent explosive resistances in both official and nongovernmental design codes for nonmilitary bridges is rarely found. Steel-concrete composite bridges have been widely adopted in urban construction for its advantages like highly construction speed and cross ability in recent years. However, the research of blast on steel-concrete composite bridge is insufficient. Therefore, it is extremely necessary to figure out the stress and failure mechanism of the steel-concrete composite bridge under blasting load.

Many researchers [1–3] focused on the structural performance of concrete piers or slabs under blasting loads. Wu et al. [4] investigated the residual capability of localized blast-damaged RC columns by LS-DYNA and the common failure mode of structures subjected to blast load and summarized the residual capacity index by a service axial load index. Yao et al. [5] investigated the damage features and dynamic response of RC beams under blasting loads. Pan et al. [6] investigated three modern types of reinforced concrete bridges under various blasting loads, including a slab-on-girder bridge, a box-girder bridge, and a long-span cable-stayed bridge and discussed the protection performance of carbon fiber-reinforced polymer on bridges. Fujikura and Bruneau [7] studied the blast resistance of steel jacketing bridge piers by experiments. Li and Hao [8] analyzed steel wire mesh-reinforced concrete slab under contact explosion.

Although the researches about bridge or other constructions under explosive listed above have obtained some results and suggestions, the research about the performance of concrete-steel composite bridges under blasting loads is still very limited. In this study, a steel-concrete composite bridge is analyzed thoroughly to obtain the damage patterns of bridge and predict propagation rule of explosive wave accurately. To do this, a three-dimensional finite element model for concrete-steel composite bridge is established by

ANSYS Autodyn. Two analysis modules, the traditional preprocessor and AUTODYN module which is professional in explosive area, are utilized in this study.

2. Material Characteristics and Modeling

2.1. Conservation Equation. Explosive process is a high-rate chemical phenomenon in which energy is released rapidly within a limited scope, which is obviously different from general structural analysis. Carta and Stochino [9] investigated the flexural failure of reinforced concrete beams under blasting loads through theoretical models, which indicated that the material constitutive relation and conservation equation have a decisive effect on the result of explosive calculation. The materials considered in this study include concrete, steel plate, ideal air, and high-explosive TNT. In order to obtain an accurate and reliable performance of the steel-concrete composite bridge under blasting loads, it is obviously necessary to simulate the behavior of explosion in air with an appropriate method. Generically, during the explosion process (usually in several milliseconds), the nearby air expands rapidly with high energy and temperature, forming a shock wave which evolves into high pressure on structure timely. The spread of shock wave in air can be described by nonviscous flow, deciding by Euler equation as follows:

$$\frac{\partial q}{\partial t}\frac{\partial f(q)}{\partial x}+\frac{\partial g(q)}{\partial y}+\frac{\partial h(q)}{\partial z}=0, \tag{1}$$

where q is the state vector about time t and $f(q)$, $g(q)$, and $h(q)$ are flux of conservative state variables.

$$q=\begin{bmatrix}\rho\\ \rho u\\ \rho\omega\\ Q\end{bmatrix},\quad f(q)=\begin{bmatrix}\rho u\\ \rho u^2+p\\ \rho uv\\ pu\omega\\ (Q+p)u\end{bmatrix},\quad g(q)=\begin{bmatrix}\rho v\\ \rho uv\\ \rho v^2+p\\ pv\omega\\ (Q+p)v\end{bmatrix},\quad h(q)=\begin{bmatrix}\rho\omega\\ \rho u\omega\\ \rho v\omega\\ p\omega^2+p\\ (Q+p)\omega\end{bmatrix}, \tag{2}$$

where ρ is the density; u, v, and ω are the velocities in the x, y, and z direction, respectively; p is the pressure; and Q is the total energy.

In order to achieve the solution, an ideal state equation is introduced by Zhou et al. [10] as follows:

$$p=(\gamma-1)\rho e, \tag{3}$$

where e is the internal energy, value of which is set to 2.068×10^8 to ensure that the structure is at a standard atmosphere pressure at the beginning of the analysis, γ is the adiabatic exponent of ideal air, and ρ is the material density. Material parameters of air are shown in Table 1.

2.2. Materials Constitutive. With an explosion taking place nearby, bridges accept a dynamic transient shock wave. Therefore, the damage of concrete occurs in a flash. To analyze and simulate the destruction of concrete under the sudden impact during explosion, the concrete failure model of Riedel–Hiermaier–Thoma is considered for concrete constitutive properties, which include elastic limit surface, failure surface, and residual strength surface. The constitutive model of RHT is shown in Figure 1.

The equation is as follows:

$$\sigma^*_{\text{eq}}(p,\theta,\varepsilon)=Y^*_{\text{TXC}}(p)R_3(\theta)F_{\text{rate}}(\dot{\varepsilon}), \tag{4}$$

where $Y^*_{\text{TXC}}(p)$ is the compressing meridian, $F_{\text{rate}}(\dot{\varepsilon})$ is the augmentation factor of strain rate, and $R_3(\theta)$ is the corner function. Researchers have shown that there are some defects in the original RHT model in spite of wide application on explosion analysis. Tu and Lu [11] modified the residual strength surface and tension meridian. Nyström and Gylltoft [12] introduced the bilinear principal tensile stress failure criterion in the RHT model. Leppänen [13] modified the tensile stress-strain relationship and tensile strength strain rate of the RHT model. In this study, the principal stress tensile failure was considered instead of original tensile failure model of RHT, value of which was set at 5.0*e*3. Crack softening option was set, and the value of fracture energy was 100. In explosive analysis, the RHT constitutive relation is usually used with the *p-alpha* state equation together. The *p-alpha* state equation is shown as follows:

$$P(\rho,E)=A_1\mu+A_2\mu^2+A_3\mu^3+(B_0+B_1\mu)\rho_0 e,\qquad \mu=\left(\frac{\rho}{\rho_0}\right)-1, \tag{5}$$

where A_1, A_2, A_3, B_0, and B_1 are calculation parameters, ρ_0 is the initial density, and e is the internal energy. The parameters are mostly obtained through experiments. In this research, Adobe 1.8-RHT is used in this analysis for its adaptability and widespread applicability from the literature. Material constitutive of steel is much more simple than concrete. Bearing steel 2.7*YS* is used in explosive analysis. Values of the parameters and other failure mechanism of these two constitutive relations are found in the literature [14].

Table 1: Material parameters of air.

ρ (g · cm^{-3})	e (J · kg^{-1})	γ
1.225$E-3$	2.068×10^8	1.4

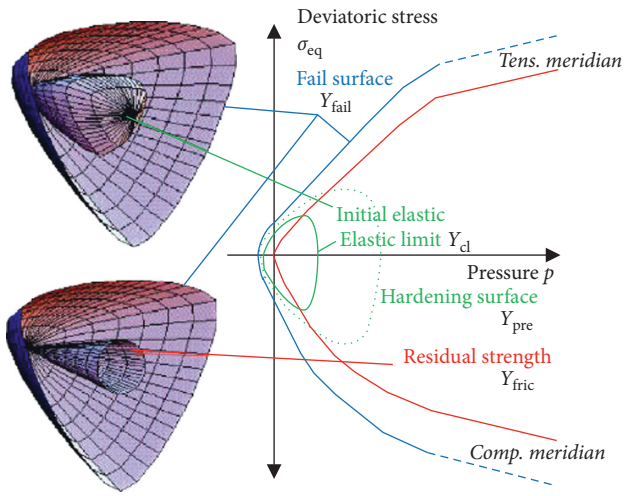

Figure 1: The RHT constitutive model used for concrete.

Jones–Wilkins–Lee (JWL) state equation is used to model to explosive material and ambient air, which can indicate the interaction between explosive pressure and air energy clearly. The air range surfaces adopt the flow-out boundary condition. The JWL equation is as follows:

$$P = A\left(1 - \frac{\omega}{R_1 V}\right)e^{-R_1 V} + B\left(1 - \frac{\omega}{R_2 V}\right)e^{-R_2 V} + \frac{\omega E_0}{V}, \quad (6)$$

where p is the pressure during explosion, V is the volume ratio of detonation products to initial explosive, E_0 is the internal energy of unit volume, and A, B, R_1, R_2, and ω are material parameters, values of which are shown in Table 2.

2.3. Finite Element Modeling. Figure 2 shows the cross section of a 40 m single span steel-concrete composite bridge whose deck width is 1250 cm. There are two I-shaped steel girders placed 670 cm apart in the bridge. Concrete bridge decks are adopted for its high pressure resistance and driving comfort. Shear studs are adopted for the connection between I-shaped steel girders and concrete deck, which is considered as ideal connection in this study. The concrete deck is fully restrained with the steel girders. The height of the box girder is 220 cm, while top plate width of I-shaped is 90 cm and bottom width is 110 cm. Transverse beams are set at every 8 meters in longitudinal directions to enhance the structural integrity. In this study, the concrete and steel girders are modeled with 8-node solid Lagrange elements and 4-node shell elements. Because of the complex nonlinearity of the macroscopic concrete, the improved Riedel–Hiermaier–Thoma (RHT) concrete failure model and the porous equation of state (EOS) model are utilized to consider the large-scale heterogeneity and porosity. Due to the complexity of structure, the three-dimensional finite element model was first established by using preprocessor module of traditional ANSYS predisposition. Explosion execution was completed in the analysis module of AUTODYN through "K file." The accuracy of the analysis is highly affected by the cell size, especially for nonlinearity multi-Euler analysis. Theoretically, a smaller mesh size of the finite element model will obtain more precise structural performance under blasting loads. However, it is infeasible to model components with unreasonable small mesh size. Pan et al. [6, 15] pointed out that a 10 cm mesh size can have an adequate assurance rate to ensure a reliable pressure-time history and dynamic structural response. The range of air is also a key factor for computational efficiency, and it is impossible to simulate an infinite space of air. A more economical approach is used to define the air flow interface. Flow-out boundary in this study is introduced for the air's free edge. Explosive analysis begins with a standard atmosphere which is achieved by defining the initial energy of air. Figure 3 shows the AUTODYN analysis model.

3. Bridge Performance and Result Discussion

Terrorist attacks and accidental explosion are always unpredictable, for which reason it is necessary to make a large number of detonation scenarios. In this study, considering the particularity of composite structure, detonation locations are the key factor of damage mode. 100 kg weight of TNT equivalent is considered for a car bomb. Above-deck and below-deck detonation are simulated in this study. Because of the instantaneity and tremendousness of explosion energy, the effect of gravity and other live load are neglected during such short period.

3.1. Above-Deck Detonation. Dynamite is located in the middle of the bridge, 80 centimeters above the deck. Figure 4 shows the wave propagation of a 100 kg weight TNT by using the three-dimensional multi-Euler domain method. The blasting wave has spread to whole lateral of the bridge system within only 6.0 milliseconds. The section at the top of the explosive shows the flow-out circumstance.

In order to illustrate the transmission rules of blast pressure on structure clearly, gauges in the air were defined to record the high blast pressure and impulse at different locations during calculation, as shown in Figure 5. Figure 6 shows the pressure history of Gauge #28, where the curve is similar to a triangle. The peak reaches 1.546$E6$ kPa, with the time corresponding to the peak value is only 1.512$E-1$ millisecond. Generally, the area of this triangle can be utilized to describe the degree of explosion. Figure 7 shows the velocity history of Gauge #28, where the air impacts down rapidly towards the bridge deck in a very short time and then is reflected. An opposite velocity can be got in the diagram. Moments later, velocity curve vibrates around the zero line.

Through the calculation results of monitoring points, the overall trends are that a smaller the pressure will be obtained with a greater distance. Figure 8 shows the pressure-time history of some gauges. Meanwhile, Gauge #16 seams have

Table 2: Material parameters of JWL equation state.

Parameter R_1	Parameter R_2	Parameter A (MPa)	Parameter B (MPa)	Parameter ω	Density ρ ($g \cdot cm^{-3}$)	V	E ($J \cdot kg^{-1}$)
4.15	0.90	3.738E5	3.747E3	0.35	1.63	1.00	7.0E6

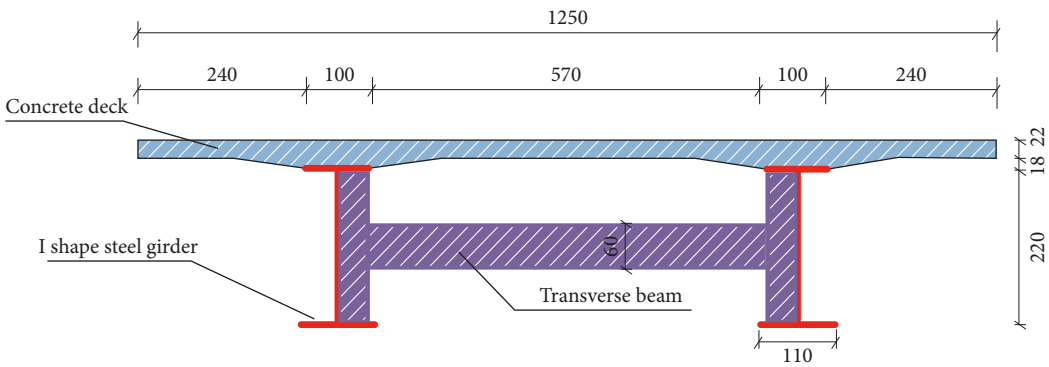

Figure 2: The cross section (unit: cm).

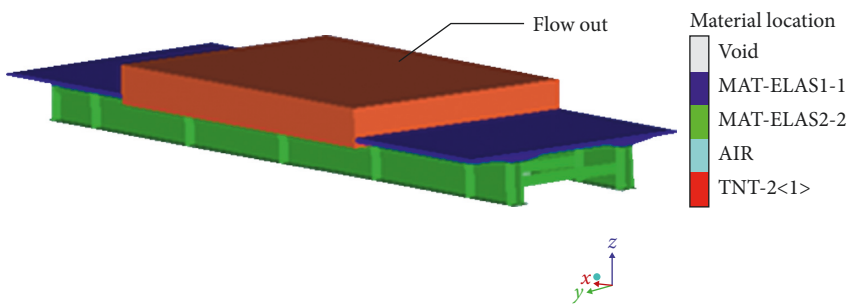

Figure 3: Analysis module in AUTODYN.

a larger pressure peak than Gauge #17, and it is due to the negative pressure phenomenon which occurs in a small distance from detonation.

Figure 9 summarizes the ultimate damage states in the case of above-deck detonation. It can be seen clearly that due to the full confinement effect and the highly reflected pressure, a 4.6 m × 4.6 m damage area was generated. The surface of the deck is predominantly damaged by direct crushing of RC elements, and at the same time, there is no damage observed in the I-shaped steel girder. Figures 10 and 11 present stress distribution. It can be seen that the blue area in the middle of the bridge reflects the quitting of concrete under blasting loads.

3.2. Below-Deck Detonation. Another situation for the urban bridge is carried out. Overpass bridges can suffer a below-deck detonation because of heavy volume of traffic below them. In this section, explosive detonation is arranged right down the composite bridge. Figure 12 presents a below-deck explosion process: explosive wave forms within a rectangle space between the I-shaped steel girders in the process of transmission.

Figure 13 shows the structure deformation under blasting loads. A large local deformation occurs in the steel girder, value of which reaches 158 mm. Because of the transverse beam, the max deformation is not in the midspan. Figure 14 shows the stress distribution on damage state. Structural failure occurs mainly in two positions: the first one is the local failure of steel girder itself and the other is the juncture position of steel girder and concrete deck.

In a similar way, Gauges are defined to figure out the stress characteristics and damage mechanism on structure. Gauges 113, 114, and 50 to 54 are arranged on the longitudinal direction and Gauges 54, 75, and 96 are arranged on the transverse direction, which is shown in Figure 15. Figure 16 shows velocity-time history of Gauges on z direction. The curve of #53 is even higher than Gauge #54 on local scale. It is because that the transverse beam right near the point limits the local deformation. Other curves of Gauge points decreased with distance. Figure 17 shows velocity-time history of Gauge points of the horizontal setting. The velocity of Gauge #75 presents some irregularity, because of the I-shaped steel beam and the local reflection effect of the explosion wave. The pressure-time history of Gauges #113 and #114 (horizontal near the detonation point) illustrates the same phenomenon. Their pressure curves cannot be simply concluded as typical triangle, and there are two peaks which are shown in Figures 18 and 19. Apparently, both failure characteristics and blasting loads below the detonation are very different from those above the detonation.

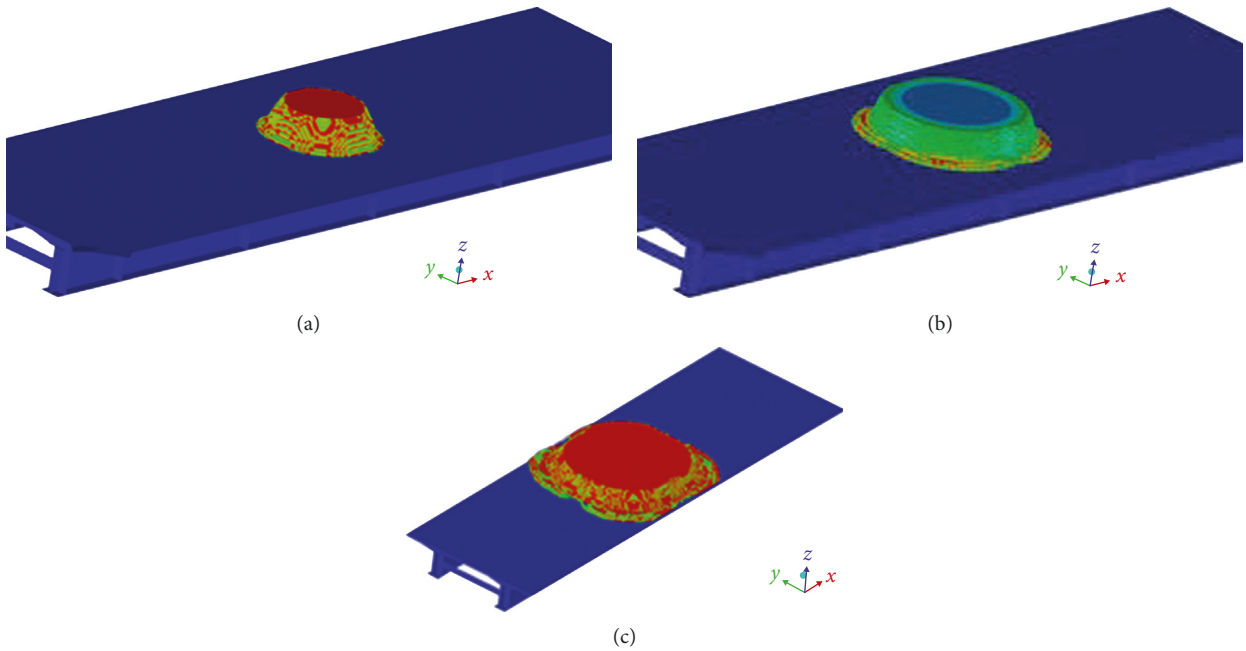

Figure 4: Blast wave spread of above-deck explosive TNT at different times: (a) 0.85 milliseconds, (b) 1.7 milliseconds, and (c) 5.99 milliseconds.

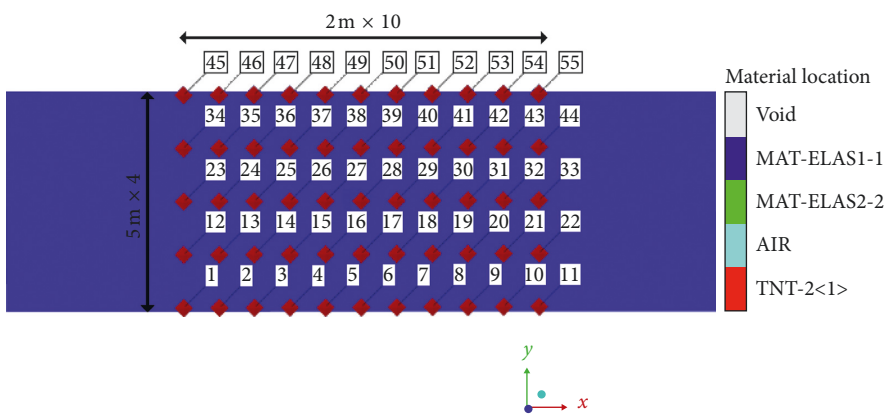

Figure 5: Defined gauges in case of above-deck detonation.

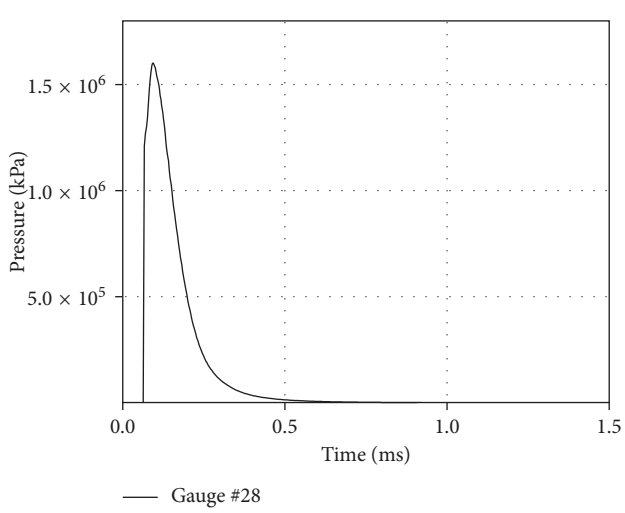

Figure 6: Pressure history of Gauge #28.

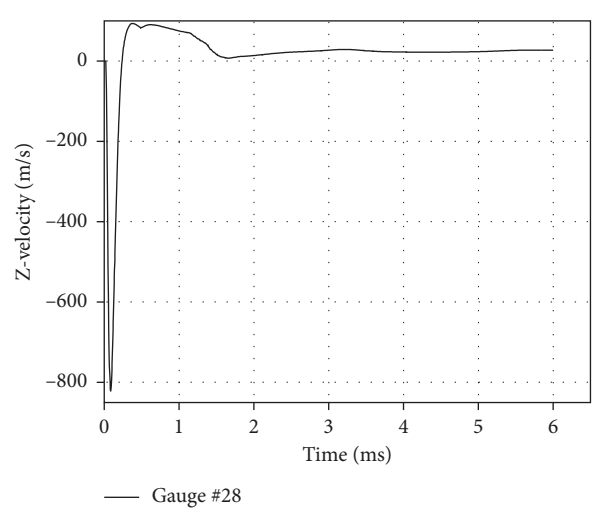

Figure 7: Velocity history of Gauge #28.

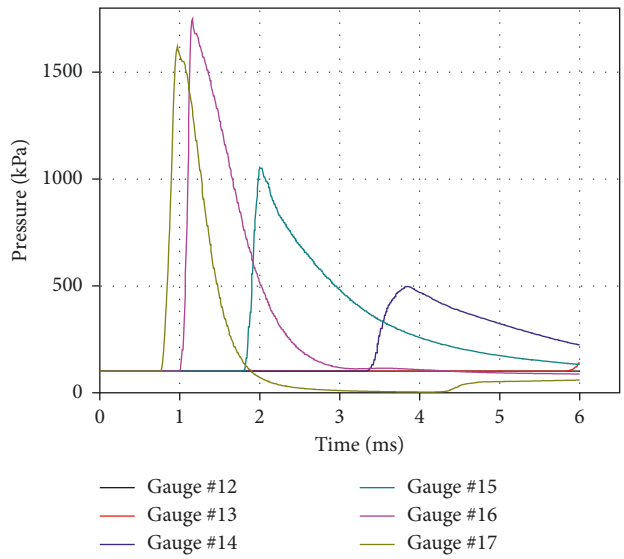

Figure 8: Pressure-time history of Gauges.

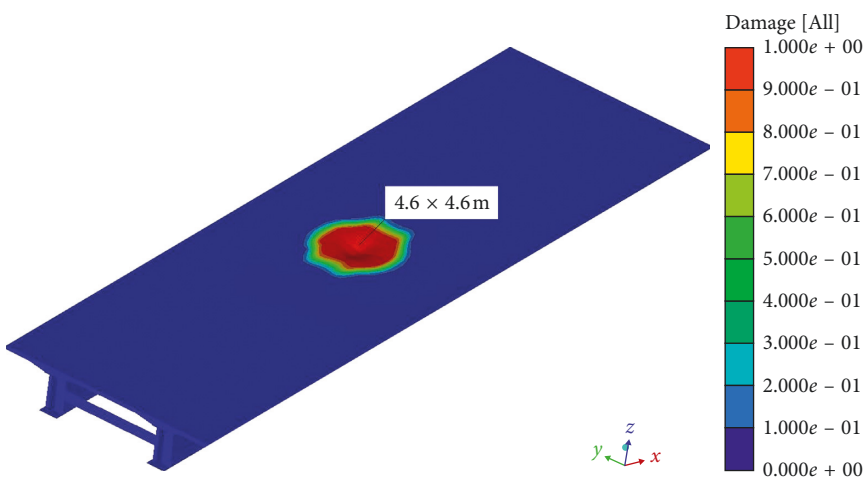

Figure 9: Damage of the bridge.

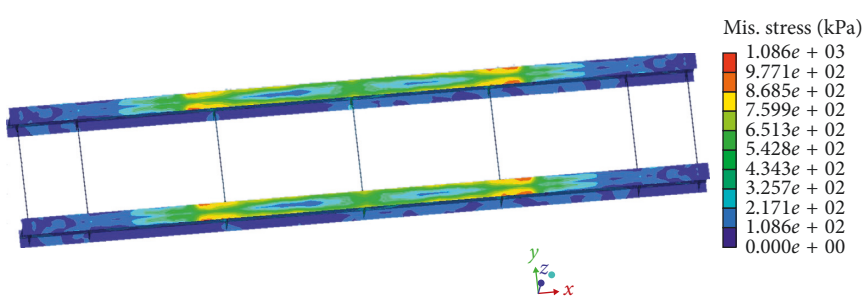

Figure 10: Stress distribution of I-shaped beam.

3.3. Discussion of Failure Characteristics. Generally, the failure characteristics of composite beam under blasting loads are dramatically influenced by detonation locations. When blast happens above the deck, the concrete of bridge deck is subjected to the impact load directly. Failure characteristics of concrete deck are similar to general failure mode, and a symmetrical area of destruction is formed, as shown in Figures 9 and 11. Meanwhile, the I steel girder bear

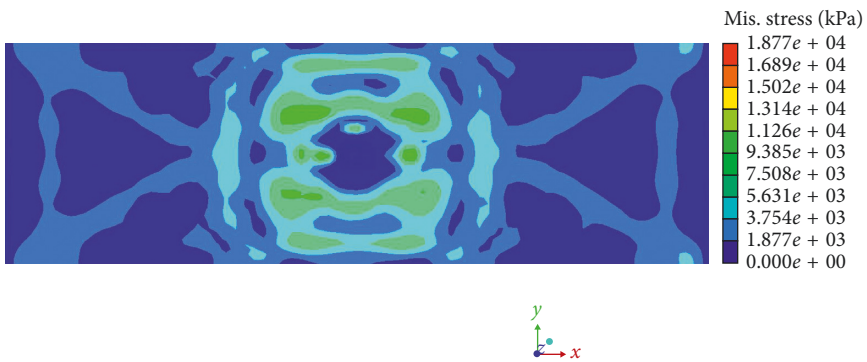

Figure 11: Stress distribution of concrete deck.

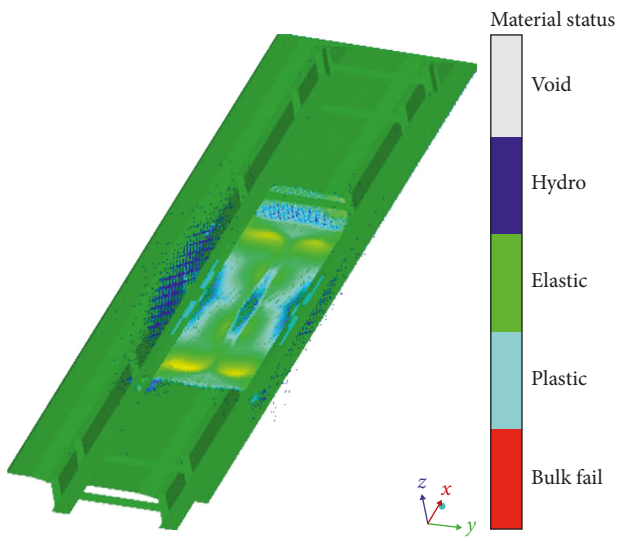

Figure 12: Blast wave spread of above-deck explosive TNT at different times.

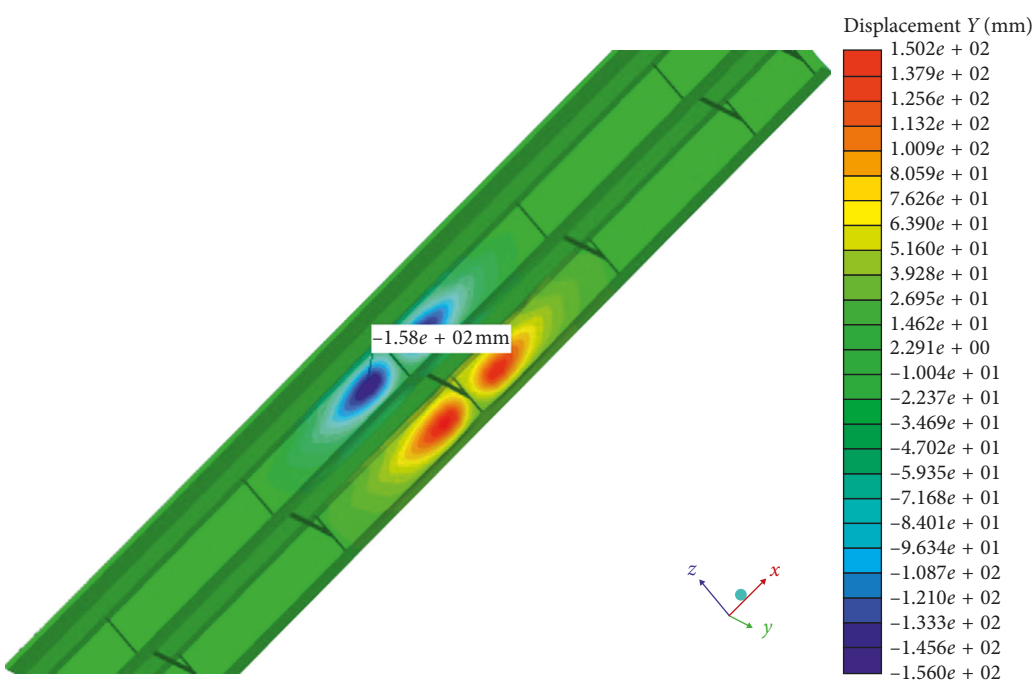

Figure 13: Deformation suffering from explosive load.

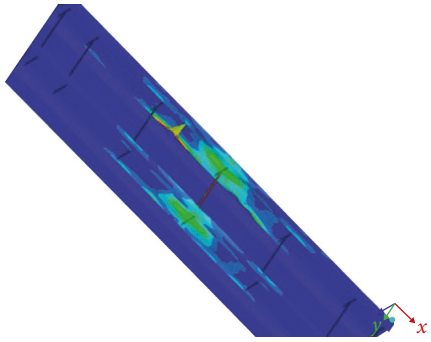

Figure 14: Stress distribution of damage state.

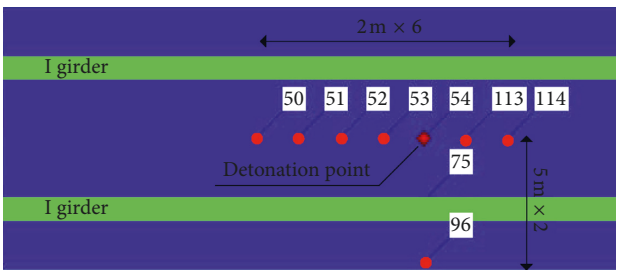

Figure 15: Defined gauges in case of down-deck detonation.

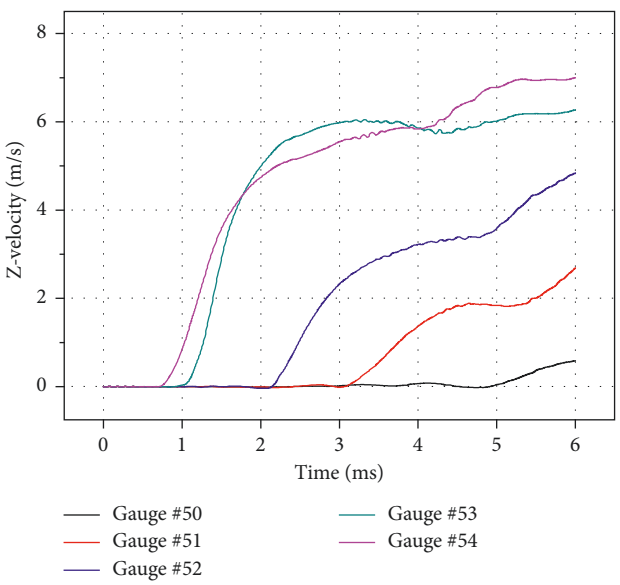

Figure 16: Velocity-time history of Gauges.

bending moments in the instant of the explosion. When explosive happens below the deck, the overpressure characteristic of the structure is more complex. Shock wave reflections are produced in local space. The overpressure time curve near the blast point showed multiple peaks, and the I-shaped girder deformed considerably.

4. Conclusions

This paper presents the blast analysis results of concrete-steel composite bridge by an accurate simulation of explosion process. The conclusions are as follows.

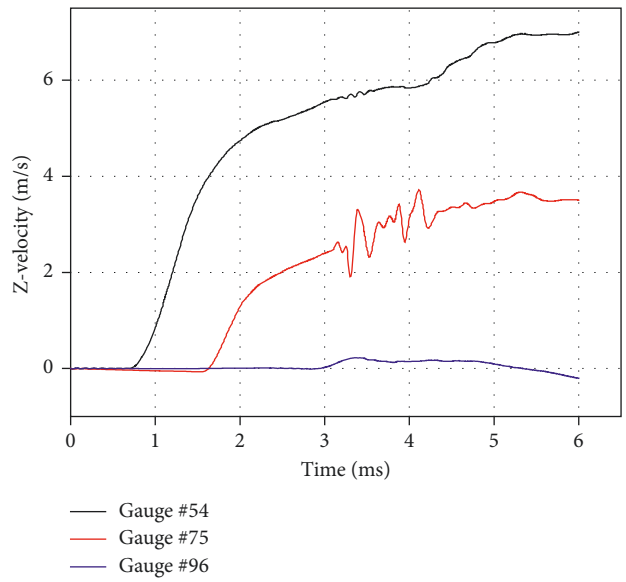

Figure 17: Velocity-time history of Gauges.

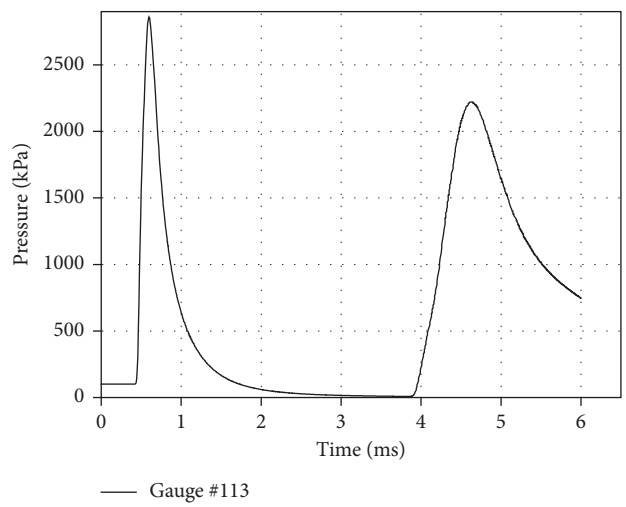

Figure 18: Velocity-time history of Gauge #113.

In the case of a steel-concrete composite bridge, a 100 kg TNT above-deck explosion right on the midspan of the bridge is identified as the most critical case. The force of explosion lead to a 4.6 × 4.6 m damage area significantly. The pressure history curve of the point right below the explosive can be described as a typical triangle because of the hollowness above the bridge deck. It means that a simple triangle time load can be utilized in explosive analysis instead of complex simulation of the whole blasting system. Arranging the detonation point at the center, it can be shown that a smaller pressure peak will be obtained with a farther distance. There is not a remarkable disruption on steel I-shaped beam.

For below-deck detonation of composite bridge, the blast propagation is more complex than that of the above-deck detonation. Blasting loads lead to more deformations and stresses for steel girder. The damage pattern mainly occurs

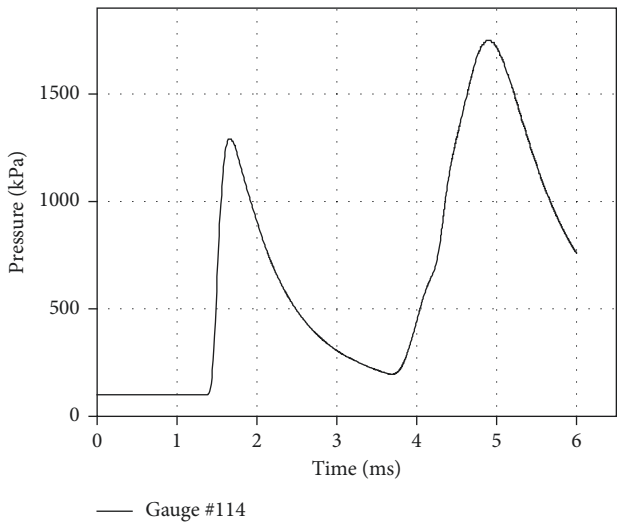

Figure 19: Velocity-time history of Gauge #114.

on two positions: steel girder near the blasting detonation and the conjunction with concrete deck and steel girder. The blast wave is also different from an ordinary open area, causing a reflection in the narrow part between the two steel girders. The pressure-time history curve is not a simple triangle, which means a simplified time load cannot be utilized to replace the actual explosive process. The transverse beam plays an important role in displacement limitation, but the overall destruction of the structure still lays on the local steel yield strength and the joint failure.

Data Availability

The data used in the manuscript can be replicated through calculation method as described in the manuscript. The data supporting the conclusions of the study can be obtained in the manuscript.

Conflicts of Interest

The authors declare that they have no conflicts of interest regarding the publication of this paper.

Acknowledgments

The authors would like to acknowledge the financial support provided by the Fundamental Research Funds for the Central Universities of China under Grant nos. 310821161012 and 300102218214. The help of engineers and technicians in the Key Laboratory of Bridge Detection Reinforcement Technology Ministry of Communications of Chang'an University is highly appreciated. These supports are gratefully acknowledged.

References

[1] Y. S. Tai, T. L. Chu, H. T. Hu, and J. Y. Wu, "Dynamic response of a reinforced concrete slab subjected to air blast load," *Theoretical and Applied Fracture Mechanics*, vol. 56, no. 3, pp. 140–147, 2011.

[2] C. F. Zhao and J. Y. Chen, "Damage mechanism and mode of square reinforced concrete slab subjected to blast loading," *Theoretical and Applied Fracture Mechanics*, vol. 63-64, pp. 54–62, 2013.

[3] S. J. Yao, D. Zhang, F. Y. Lu, W. Wang, and X. G. Chen, "Damage features and dynamic response of RC beams under blast," *Engineering Failure Analysis*, vol. 62, pp. 103–111, 2016.

[4] K. C. Wu, B. Li, and K. C. Tsai, "Residual axial compression capacity of localized blast-damaged RC columns," *International Journal of Impact Engineering*, vol. 38, no. 1, pp. 29–40, 2011.

[5] S. J. Yao, D. Z. Zhang, X. G. Chen, F. Y. Lu, and W. Wang, "Experimental and numerical study on the dynamic response of RC slabs under blast loading," *Engineering Failure Analysis*, vol. 66, pp. 120–129, 2016.

[6] Y. X. Pan, C. E. Ventura, and M. M. S. Cheung, "Performance of highway bridges subjected to blast loads," *Engineering Structures*, vol. 151, pp. 788–801, 2017.

[7] S. Fujikura and M. Bruneau, "Experimental investigation of seismically resistant bridge piers under blast loading," *Journal of Bridge Engineering*, vol. 16, no. 1, pp. 63–71, 2011.

[8] J. Li and H. Hao, "Numerical study of concrete spall damage to blast loads," *International Journal of Impact Engineering*, vol. 68, pp. 41–55, 2014.

[9] G. Carta and F. Stochino, "Theoretical models to predict the flexural failure of reinforced concrete beams under blast loads," *Engineering Structures*, vol. 49, pp. 306–315, 2013.

[10] X. Q. Zhou, V. A. Kuznetsov, H. Hao, and J. Waschl, "Numerical prediction of concrete slab response to blast loading," *International Journal of Impact Engineering*, vol. 35, no. 10, pp. 1186–1200, 2008.

[11] Z. G. Tu and Y. Lu, "Modifications of RHT material model for improved numerical simulation of dynamic response of concrete," *International Journal of Impact Engineering*, vol. 37, no. 10, pp. 1072–1082, 2010.

[12] U. Nyström and K. Gylltoft, "Comparative numerical studies of projectile impacts on plain and steel-fibre reinforced concrete," *International Journal of Impact Engineering*, vol. 38, no. 2-3, pp. 95–105, 2011.

[13] J. Leppänen, "Concrete subjected to projectile and fragment impacts: modelling of crack softening and strain rate dependency in tension," *International Journal of Impact Engineering*, vol. 32, no. 11, pp. 1828–1841, 2006.

[14] C. Sauer, A. Heine, and W. Riedel, "Developing a validated hydrocode model for adobe under impact loading," *International Journal of Impact Engineering*, vol. 104, pp. 164–176, 2017.

[15] Y. X. Pan, B. Y. B. Chan, and M. M. S. Cheung, "Blast loading effects on an RC slab-on-girder bridge superstructure using the multi-Euler domain method," *Journal of Bridge Engineering*, vol. 18, no. 11, pp. 1152–1163, 2013.